Evaporation-Triggered Wetting Transition for Water Droplets upon Hydrophobic Microstructures

Peichun Tsai,[1,*] Rob G. H. Lammertink,[2] Matthias Wessling,[2] and Detlef Lohse[1]

[1]*Physics of Fluids Group, Faculty of Science and Technology, Impact and Mesa+ Institutes, University of Twente, P.O. Box 217 7500AE Enschede, The Netherlands*

[2]*Membrane Science and Technology Group, Faculty of Science and Technology, Impact and Mesa+ Institutes, University of Twente, P.O. Box 217 7500AE Enschede, The Netherlands*

(Received 24 September 2009; published 18 March 2010)

When placed on rough hydrophobic surfaces, water droplets of diameter larger than a few millimeters can easily form pearls, as they are in the Cassie-Baxter state with air pockets trapped underneath the droplet. Intriguingly, a natural evaporating process can drive such a Fakir drop into a completely wetting (Wenzel) state. Our microscopic observations with simultaneous side and bottom views of evaporating droplets upon transparent hydrophobic microstructures elucidate the water-filling dynamics and suggest the mechanism of this evaporation-triggered transition. For the present material the wetting transition occurs when the water droplet size decreases to a few hundreds of micrometers in radius. We present a general global energy argument which estimates the interfacial energies depending on the drop size and can account for the critical radius for the transition.

DOI: 10.1103/PhysRevLett.104.116102 PACS numbers: 68.08.Bc

In nature some plants with microstructured waxy leaves keep themselves dry and clean against rain or pesticide droplets [1]. The hydrophobic, rough or even microstructured surfaces suspend tiny liquid drops with air being trapped in between the droplets and the surface. This so-called Cassie-Baxter (CB) or ''Fakir'' state [2] possesses a large contact angle and sometimes is highly disadvantageous in industrial applications, such as printing, coating, spraying, and sputtering processes. In contrast, in microfluidic applications the CB state is desirable to allow for slip and thus an enhanced flow rate [3]. In this Letter, we demonstrate that an evaporation process can drive the transition from a Fakir droplet to a homogeneous wetting state, i.e., to the Wenzel (W) state. We explain the underlying mechanism by an energy balance argument.

The deceptively simple process of a freely evaporating droplet on a solid surface can produce various intriguing patterns, such as coffee stains [4] and wine tears [5]. These patterns are consequences of the complex interplay between several physical processes: mass, heat and energy exchange across different interfaces, diffusive and convective flows, possible Marangoni circulations [6] in the presence of a temperature or concentration gradient, and the movement of the triple line [7]. Yet, most investigations of evaporating droplets are conducted with hydrophilic and hydrophobic flat surfaces [8–12], and rarely with ultrahydrophobic patterned substrates [13–15].

Figure 1 shows the experiment of a freely evaporating water droplet placed on a hydrophobic micropatterned substrate. The surface is composed of PDMS (Polydimethylsiloxane) microstructures, thereby being transparent and ultrahydrophobic. The precisely controllable microstructures were realized via a micromolding technique. The sample preparation includes mixing and then degassing the PDMS component A with the curing agent B (10:1 mass ratio, Dowcorning Sylgard elastomer). The mixture is cast onto a hydrophobized wafer with desired micropatterns and finally heated in an oven at 85° for 3 hours. The SEM picture in Fig. 1 shows the substrate, which consists of regular micron-sized pillars of width w, height h, and interspace a in a square lattice with a periodicity $d = w + a$. In the experiments $w = 5\ \mu$m, $a = 5\ \mu$m, and h is varied between 6, 10, and 20 μm to investigate the geometric effect on the wetting transition. Our micropillars are densely packed, with an area packing fraction of the solid pillars $\Phi_s = w^2/d^2 = 0.25$ ($\Phi_s = \pi w^2/4d^2 \simeq 0.20$) for rectangular (cylindrical) shaped pillars in a square lattice, where Φ_s is the ratio of the solid to the total cross section areas. The contact angle on the flat PDMS surface, θ_f, was measured to be $(113 \pm 7)°$.

The evaporation process was carried out at room temperature (21 ± 1) °C with a relative humidity of $35 \pm 5\%$. The used liquid was ultrapurified milli-Q water with different initial drop sizes, 2–3 mm in diameter. The side-view images of the evaporating drop were captured via

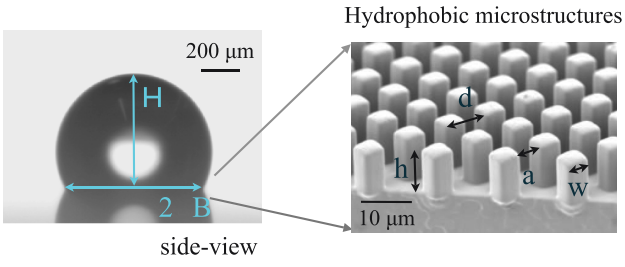

FIG. 1 (color online). Experiment of an evaporating water droplet on a hydrophobic microstructured surface shown by the SEM (scanning electron microscope) image on the right.

4–20× magnifying lenses with a CCD camera using the recording rate of 1–2 fps (frame per second). The temporal variations of drop height H and base diameter $2B$ were measured. Simultaneously, the sample was observed using an inverted microscope (Axiovert 40 CFL, Carl Zeiss BV). The bottom-view images were recorded through the translucent polymeric substrate with a high speed camera at 50–10 000 fps via an objective of 10 or 20× magnification. The highest spatial resolution is about 1 μm/pixel. The snapshots of the bottom views facilitate the investigation of the water infiltration dynamics and the accurate measurement of the critical base radius B_c at the wetting transition.

Figure 2 illustrates representative water impaling dynamics at the evaporation-triggered CB to W wetting transition (1st frame) and beyond up to the fully wetting state (last frame). In the Fakir state, prior to the transition we observe the perimeter of the contact line globally resembles a circular shape while locally adapting to the microsquare lattice. During the evaporation the triple contact line advances in a stepwise manner, corresponding to the periodicity d of the microstructures. We noticed that the shape of the droplet base at the critical point is mostly circular for tall micropillars ($h = 10$ and 20 μm). Polygonal or irregular base shapes were seen for short pillars ($h = 6$ μm). The infiltration point (see arrow in Fig. 2) mostly ($\approx 93\%$ based on 28 experiments) occurs at the edge of the water base, i.e., close to the contact line.

The water invading dynamics, as shown in Fig. 2, reflects the geometric arrangement of the micropillars and presents two rather different time scales for the water propagation. The wetted area is shown by the dark region with a square edge at the right upper corner, while the left bottom corner is constrained by the circular contact line. The water front first locally advances into one row and then quickly zips to the side perpendicular to the front direction.

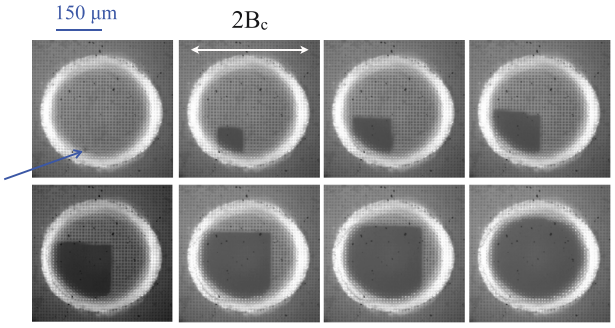

FIG. 2 (color online). Snapshots of the bottom view reveal the water infiltration dynamics at the transition from a Cassie-Baxter to a Wenzel wetting state triggered by evaporation. Here, the microstructures are arranged in a square lattice with a dimension of $a = 5$, $w = 5$, and $h = 10$ μm. The dark areas indicate the water imbibition, while the air pockets present in the bright areas enclosed by a rather bright circumference marked by the droplet base. These images are sequentially recorded at $t = 0$, 30, 58, 72, 116, 180, 236 and 310 ms from the transitional point, determined by the first frame where a small initial infiltration point is observed (marked by an arrow).

The water front propagated with a mean speed of 0.65 mm/s while the fast zipping speed was about 8× faster. The same kind of water impaling dynamics has been observed and more detailedly investigated with a variety of polymeric microstructures, though, at a spontaneous or a pretriggered wetting transition [16–18]. Pronounced geometric effects on the water imbibition exist for both hydrophobic [16] and hydrophilic micropillars [19].

Complimentary to the bottom views, side-view images as shown in Fig. 3 also provide useful information on the contact angle dynamics. Figure 4(a) shows the change of the macroscopic contact angle θ_{CA} in the course of the evaporation. θ_{CA} was calculated from the measurements of H and B by assuming a spherical water cap. A kink after which a steep decrease in θ_{CA} can be noticed marks the wetting transition [$*$ in Fig. 4(a)], while both H and B gradually decrease in time [see the inset of Fig. 4(a)]. Figure 4(b) shows the curvature radius R of the evaporating droplet. R first decreases in time with a power-law relation and then increases again after the wetting transition. The red line is the best fit of the power law $R(t) = C(t_f - t)^{\alpha}$, with the fitting results of $t_f = 505.7$ s and $\alpha = 0.61$. This power law fits well the radius of the CB state and could be used to estimate t_f, if there were no transition to the Wenzel state (however, there is such a transition). In comparison, for a pure diffusive evaporation, ignoring thermal and Marangoni convections, the evaporation rate is proportional to the perimeter of the droplet and the exponent then should be 1/2 [4]. Indeed, experiments with a variety of completely wetting liquids of alkanes drying on flat, isothermal, smooth, wetting surfaces found exponents close to 1/2 [11], suggesting a diffusive evaporation process for these completely wetting liquids. However, for an evaporating water droplet the exponent $\alpha \approx 0.60$ has been observed down to the drop radius ≈ 500 μm on a flat and perfectly wetting surface, such as mica, with different humidities and temperature [12]. These observations might suggest a universal scaling for a naturally evaporating water droplet with a freely moving contact line. More importantly, in Fig. 4(b) the data deviate from this

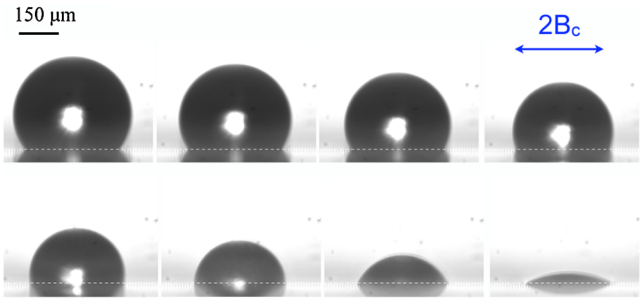

FIG. 3 (color online). Snapshots of the side views of an evaporating droplet with the time interval 15 s between the images, revealing the decrease of the contact angle. The dashed lines, marking the drop base, separate the main droplet from its mirror image. The arrow shows the length scale of the critical diameter $2B_c$ at the wetting transition, determined from the bottom views.

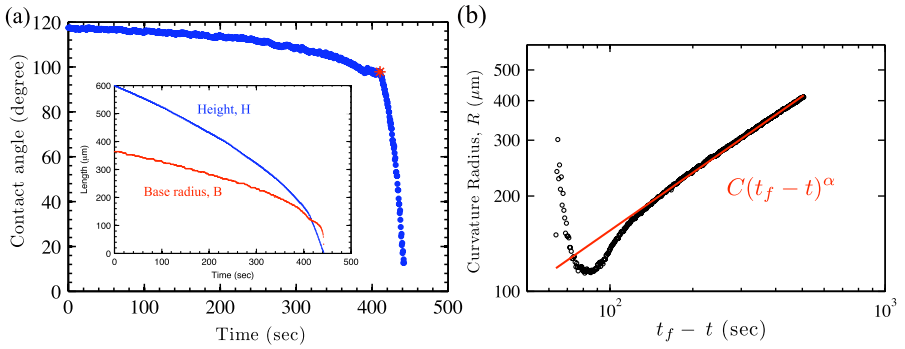

FIG. 4 (color online). (a) A typical contact angle dynamic of a water droplet evaporating on hydrophobic microstructure substrates of regular pillars of the width $w = 5$ μm, the interspacing $a = 5$ μm, and height $h = 6$ μm in a square lattice. The contact angle is calculated with the time evolutions of the drop height H and the base radius B, shown in the inset, by assuming a spherical cap. The symbol $*$ marks the transition point from CB to W state. (b) The corresponding curvature radius R reveals a power law in time for $R \gtrsim 200$ μm. The red line shows the best scaling fit of $C(t_f - t)^\alpha$, with the power-law exponent $\alpha = 0.61$.

power-law relation for droplet radii smaller than 200 μm in the Wenzel transition state with the triple line pinned.

How to predict the critical drop size at the CB to W transition triggered by natural evaporation? Recent studies have proposed two different mechanisms for the transition, namely, the ''touch-down'' and the ''pinning instability'' scenarios [20–22]. The touch-down model assumes that the contact lines of the drop remain pinned on the top edges of the pillars [20,21]. As the radius of the evaporating droplet gets smaller, the local Laplace pressure enlarges and thus drives the menisci to protrude deeper. The meniscus depth δ grows according to $\delta \sim a^2/R$ [20]. The CB to W transition occurs when δ reaches the bottom of the pillars, i.e., when $\delta = h$, resulting in the critical radius $R^* \approx a^2/h \approx 5$ μm for our experimental parameters. The pinning instability scenario describes the depinning of the contact lines. Instability sets in once the angle α between the meniscus and the pillar side is larger than the contact angle θ_f [20]. The resulting prediction of the critical radius is $R^* \sim a/|\cos(\theta_f)| \approx 13$ μm for our experimental conditions. Alternatively, a sufficiently large Laplace pressure can also drive menisci to slide down along the sides of the pillars, as described by Eqn. (3) of Ref. [22], which gives $R^* \approx 10$ μm for our geometric parameters. All three of these predictions do not agree with our result $R^* \sim B^* \sim$ 100–250 μm. Therefore, for an alternative explanation of this observed critical size, we now develop a new argument, based on the global surface energies E_{CB} and E_W for the CB and the Wenzel states.

The total surface energy E_{CB} (E_W) is the sum of all energies needed for creating interfaces when placing a Fakir (Wenzel) drop onto the microstructures. During the evaporation, the drop size slowly changes with time and thus E_{CB} and E_W depend on size. The three interfacial tensions are denoted σ_{ls}, σ_{sg}, and σ_{lg} for the liquid-solid, solid-gas, and liquid-gas interfaces, respectively. Assuming flat menisci, $E_{\mathrm{CB}} = N[\sigma_{\mathrm{ls}} w^2 + \sigma_{\mathrm{sg}}(4wh + d^2 - w^2) + \sigma_{\mathrm{lg}}(d^2 - w^2)] + \sigma_{\mathrm{lg}} S_{\mathrm{cap}}$, where N is the number of asperities underneath the droplet base, and S_{cap} is the surface area of the water cap entirely in contact with the air. Similarly, $E_W = N[\sigma_{\mathrm{ls}}(d^2 + 4wh)] + \sigma_{\mathrm{lg}} S_{\mathrm{cap}}$. According to our experimental condition, we used $\sigma_{\mathrm{lg}} = 70m$ N/m for the surface tension of water and $\sigma_{\mathrm{sg}} = 25m$ N/m for the PDMS surface [23]. We then estimated the interfacial tension σ_{ls} between water and the PDMS surface by a force balance at the triple line. This is equivalent to the Young's relation: $\sigma_{\mathrm{lg}} \cos\theta_{\mathrm{CA}} = \sigma_{\mathrm{sg}} - \sigma_{\mathrm{ls}}$, where θ_{CA} is the macroscopic contact angle. The dependence of the contact angle on the contact line curvature $1/B$ indicates a change of the liquid pressure at the three-phase contact line and thus a variation of the adsorption at the solid-liquid interface, thereby consequently changing the interfacial tension σ_{ls} between solid and liquid [24]. The change of contact angle during a natural evaporation has been measured numerously for hydrophilic [10,11,25], hydrophobic [9] (and the references therein) and, to a less extent, for superhydrophobic surfaces [8,13,14]. Yet, for superhydrophobic samples very limited data have been reported in the literature and no rigorous theory has been developed for the contact angle evolution during evaporation. We used the experimental data of droplet height H and base radius B from the side views to obtain the dependence of θ_{CA} on droplet size by assuming a spherical cap for the water droplet.

Figure 5 shows a representative calculation of the total surface energy, depending on the drop size, for the CB and W state. When the base radius is large, $B \gtrsim 150$ μm, the CB state is energetically favorable with a lower value of E_{CB} than E_W. The inset of Fig. 5 shows the energy difference $\Delta E = E_{\mathrm{CB}} - E_W$. For the wetting transition it holds $\Delta E(B^*) = 0$, giving the critical base radius B^*. In this case, the predicted critical value of base radius is $B^* = 123$ μm, which is in a good agreement with the experimental result $B_c = 125$ μm, determined from the bottom images.

We now extend our energy argument to various microstructures of different geometric arrangements. Figure 6 shows the critical base radius for micropillars of different h and pillar shapes (round or square), which can yield different surface roughness and packing fraction. The energy

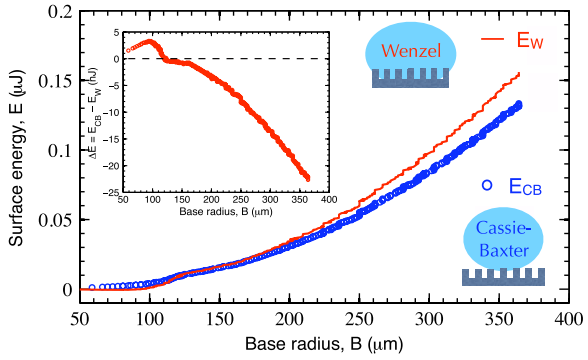

FIG. 5 (color online). Representative global interfacial energies of the Cassie-Baxster and Wenzel states: E_{CB} and E_W, respectively, as a function of drop size. The inset shows the difference of these two energies, $\Delta E = E_{\mathrm{CB}} - E_W$, giving the critical base radius B^* for the wetting transition when $\Delta E = 0$.

estimate that predicts B^* agrees very well with the critical size B_c obtained from the bottom views. As discussed before, the data presented here with densely packed pillars do not agree well with the predictions by the ''pinning instability'' model and by the touch-down scenario, which predicts a linear increase of B^* with the geometric parameter a^2/h. Instead, they agree well with our proposed global interfacial energy model.

In summary, we experimentally monitored simultaneous side and bottom views of evaporating water droplets placed on hydrophobic micropatterns. The most essential observation is the change of the macroscopic contact angle during evaporation as the droplet gradually gets smaller and smaller. At a certain size (B^* a couple of 100 μm) the initial water Fakir droplet jumps into the then energetically favorable Wenzel state. At the transition, the water infiltration dynamics starts at some nucleus and then propagates in a stepwise manner, which is profoundly affected by the geometric arrangements of the micropillars, in spite of the

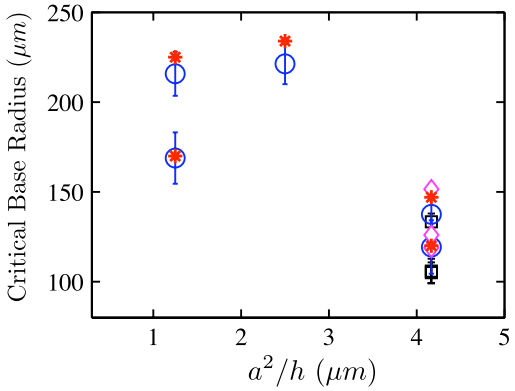

FIG. 6 (color online). The critical base radius at the evaporation-triggered CB to W transition vs the geometric parameter, a^2/h, for different initial droplet sizes. Experimental data for B_c, marked by ○ (□) for cylindrical (squared) micropillars in a squared lattice, agree well with the predicted B^* shown by ∗ (◇) using the presented energy argument for the cylindrical (squared) micropillars.

pinned triple line. The successful predictions of the critical radius by the global interfacial energy argument is remarkable, as the transition from the CB to the W state is first only local.

The authors gratefully thank Jacco Snoeijer for stimulating discussion, Alisia M. Peters for the micropatterned molds, and the IMPACT institute for financial support.

*Corresponding author.

[1] C. Neinhuis and W. Barthlott, Ann. Bot. **79**, 667 (1997).
[2] A. B. D. Cassie and S. Baxter, Trans. Faraday Soc. **40**, 546 (1944).
[3] E. Lauga and H. A. Stone, J. Fluid Mech. **489**, 55 (2003).
[4] R. D. Deegan, O. Bakajin, T. F. Dupont, G. Huber, S. R. Nagel, and T. A. Witten, Nature (London) **389**, 827 (1997); R. D. Deegan, Phys. Rev. E **61**, 475 (2000).
[5] A. Hosoi and J. Bush, J. Fluid Mech. **442**, 217 (2001).
[6] L. E. Scriven and C. V. Sterning, Nature (London) **187**, 186 (1960).
[7] J. L. Plawsky, M. Ojha, A. Chatterjee, and P. C. Wayner, Jr, Chem. Eng. Commun. **196**, 658 (2009).
[8] D. H. Shin, S. H. Lee, J.-Y. Jung, and J. Y. Yooc, Microelectron. Eng. **86**, 1350 (2009)
[9] H. Y. Erbil, G. McHale, S. M. Rowan, and M. I. Newton, Langmuir **15**, 7378 (1999).
[10] H. Y. Erbil, G. McHale, and M. I. Newton, Langmuir **18**, 2636 (2002).
[11] M. Cachile, O. Bénichou, C. Poulard, and A. Cazabat, Langmuir **18**, 8070 (2002).
[12] N. Shahidzadeh-Bonn, S. Rafaï, A. Azouni, and D. Bonn, J. Fluid Mech. **549**, 307 (2006).
[13] G. McHale, S. Aqil, N. J. Shirtliffe, M. I. Newton, and H. Y. Erbil, Langmuir **21**, 11053 (2005).
[14] X. Zhang, S. Tan, N. Zhao, X. Guo, X. Zhang, Y. Zhang, and J. Xu, Chem. Phys. Chem. **7**, 2067 (2006).
[15] Y. C. Jung and B. Bhushan, J. Microsc. **229**, 127 (2008).
[16] M. Sbragaglia, A. M. Peters, C. Pirat, B. M. Borkent, R. G. H. Lammertink, M. Wessling, and D. Lohse, Phys. Rev. Lett. **99**, 156001 (2007).
[17] C. Pirat, M. Sbragaglia, A. M. Peters, B. M. Borkent, R. G. H. Lammertink, M. Wessling, and D. Lohse, Europhys. Lett. **81**, 66 002 (2008).
[18] A. M. Peters, C. Pirat, M. Sbagaglia, B. M. Borkent, M. Wessling, R. G. H. Lammertink, and D. Lohse, Eur. Phys. J. E **29**, 391 (2009).
[19] L. Courbin, E. Denieul, E. Dressaire, M. Roper, A. Ajdari, and H. A. Stone, Nature Mater. **6**, 661 (2007).
[20] M. Reyssat, J. M. Yeomans, and D. Quéré, Europhys. Lett. **81**, 26 006 (2008).
[21] H. Kusumaatmaja, M. L. Blow, A. Dupuis, and J. M. Yeomans, Europhys. Lett. **81**, 36 003 (2008).
[22] S. Moulnet and D. Bartolo, Eur. Phys. J. E **24**, 251 (2007).
[23] P. G. de Gennes, F. Brochard-Wyart, and D. Quéré, *Capillarity and Wetting Phenomena* (Springer, New York, 2004).
[24] C. A. Ward and J. Wu, Phys. Rev. Lett. **100**, 256103 (2008).
[25] G. Guéna, C. Poulard, and A. Cazabat, Appl. Math. Res. Express **2006**, 23465 (2006).